Chemically Doped Double-Walled Carbon Nanotubes: Cylindrical Molecular Capacitors

Gugang Chen,[1] S. Bandow,[4] E. R. Margine,[1] C. Nisoli,[1] A. N. Kolmogorov,[1] Vincent H. Crespi,[1] R. Gupta,[1] G. U. Sumanasekera,[3] S. Iijima,[4,5] and P. C. Eklund[1,2,*]

[1]*Department of Physics, The Pennsylvania State University, University Park, Pennsylvania 16802, USA*
[2]*Department of Materials Science, The Pennsylvania State University, University Park, Pennsylvania 16802, USA*
[3]*Department of Physics, University of Louisville, Louisville, Kentucky 40292, USA*
[4]*Department of Materials Science and Engineering, Meijo University, Nagoya 468-8502, Japan*
[5]*Japan Science and Technology Corporation , NEC Corporation, Tsukuba 305-8501, Japan*

(Received 20 December 2002; published 25 June 2003)

A double-walled carbon nanotube is used to study the radial charge distribution on the positive inner electrode of a cylindrical molecular capacitor. The outer electrode is a shell of bromine anions. Resonant Raman scattering from phonons on each carbon shell reveals the radial charge distribution. A self-consistent tight-binding model confirms the observed molecular Faraday cage effect, i.e., most of the charge resides on the outer wall, even when this wall was originally semiconducting and the inner wall was metallic.

DOI: 10.1103/PhysRevLett.90.257403 PACS numbers: 78.30.Na, 78.67.Ch

Nanometer-scale capacitive charging effects are already familiar, e.g., the Coulomb blockade phenomenon in quantum dots. However, it is difficult to resolve the detailed radial charge distribution within a nanostructure. Using bromine-doped double-walled carbon nanotubes (DWNTs), we have resolved the radial charge distribution within the positive carbon electrode of a multilayered molecular capacitor. The walls of a DWNT are weakly coupled and so maintain distinct resolvable vibrational modes, even when they are in intimate electrical contact. The bromine acts as a ''radial gate'' with very different band filling effects on each shell and nanoscale electrostatics dominates over quantum confinement. The high-frequency Raman-active vibrations of sp^2 carbon (e.g., solid C_{60} or graphite) are sensitive to chemical doping [1–3]. The C-C bond contracts (expands) for acceptor (donor) [1,2,4], as seen in electrochemically intercalated graphite-H_2SO_4 compounds via neutron diffraction [5]. Single-walled carbon nanotubes (SWNTs) can be doped either p or n type [6–8]. The DWNT is the latest well-ordered all-carbon structure to be found [9], following fullerenes, multiwalled and single-walled carbon nanotubes (MWNT, SWNT) [10], nanohorns [11], and peapods [9,12,13]. The DWNTs studied here were made by a high temperature coalescence of C_{60} peas within peapods (C_{60}@$[n, m]$) [9]. Our peapod sample has a filling factor close to 100%, as estimated from TEM observation [14] and x-ray diffraction (XRD) profiles [15], with a shell spacing (0.36 nm) close to that in graphite [9,16].

Resonant Raman scattering is a powerful probe of both SWNT and DWNT systems [9,16–18]. Previous reports indicate that bromine can either chemically dope SWNTs and MWNTs [4] or form a C-Br complex [19]. In this work, *in situ* Raman spectra of bundled SWNT and DWNT samples during vapor phase bromine doping were acquired through the walls of a glass ampoule connected to a separate liquid bromine source. Self-supporting DWNT or SWNT films were placed in an evacuated glass tube via a valve connected to a bulb of frozen bromine. Doping occurred as the bromine warmed slowly to room temperature. The SWNT comparison spectra came from the same starting material that was used to synthesize the DWNTs.

The Raman spectra in Fig. 1 show the low-frequency radial breathing modes (RBMs) [Fig. 1(a)] and the high-frequency tangential (T) modes [Fig. 1(b)] for pristine and bromine-doped DWNT samples, collected with a Bomem DA3+ spectrometer (1 cm^{-1} resolution). Consistent with previous Raman results [16] and band structure calculations [20,21], the incident photon (1064 nm) can resonate with E_{22}^s in the outer semiconducting tubes and E_{11}^s in the inner semiconducting tubes simultaneously, where E_{ii} is the energy difference between filled and empty Van Hove singularities [2]. In the pristine DWNT sample, three low-frequency and three high-frequency RBMs are observed and assigned to the most dominant outer ($d \approx 1.45$, 1.33, and 1.26 nm) and inner shells ($d \approx 0.75$, 0.70, and 0.68 nm) using the expression $\omega_{\mathrm{RBM}}(\mathrm{cm}^{-1}) = 234/d(\mathrm{cm\,nm}^{-1})$ [16]. The proportionality constant (234 cm^{-1} nm) is an average over several literature values [16]. Small changes in ω_{RBM} due to sp^2/sp^3 hybridization in the inner shell would induce small deviations from this $1/d$ form, without affecting our main conclusions. Although the scattering from the RBMs of the outer tube is extinguished by bromine doping, the signal from the inner tube is essentially unaffected. Note that we do not see the 260 cm^{-1} peak reported earlier in bromine saturation doped SWNT bundles [4]. In the present work, we took ~100 spectra, one every few minutes during an *in situ* experiment. As the RBMs begin to up-shift with bromine doping, the intensity drops quickly. The extinction of the outer tube radial breathing band may be due to the loss of Raman

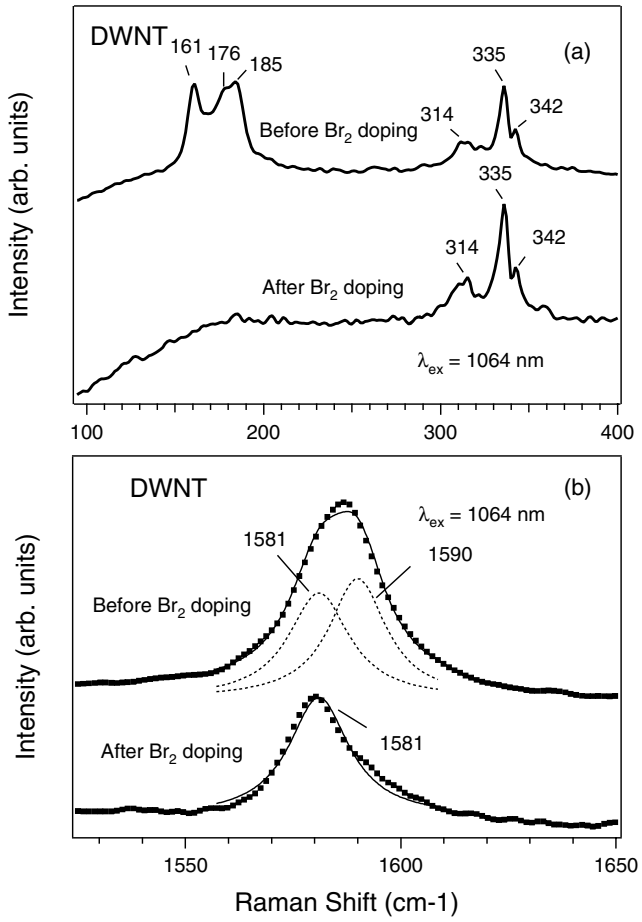

FIG. 1. Unpolarized Raman scattering spectra ($T = 300$ K) of DWNTs using 1064 nm laser excitation: (a) low frequency radial modes and (b) high frequency tangential modes. The thin solid line is the fit to the spectrum, with Lorentzian components represented by dashed lines.

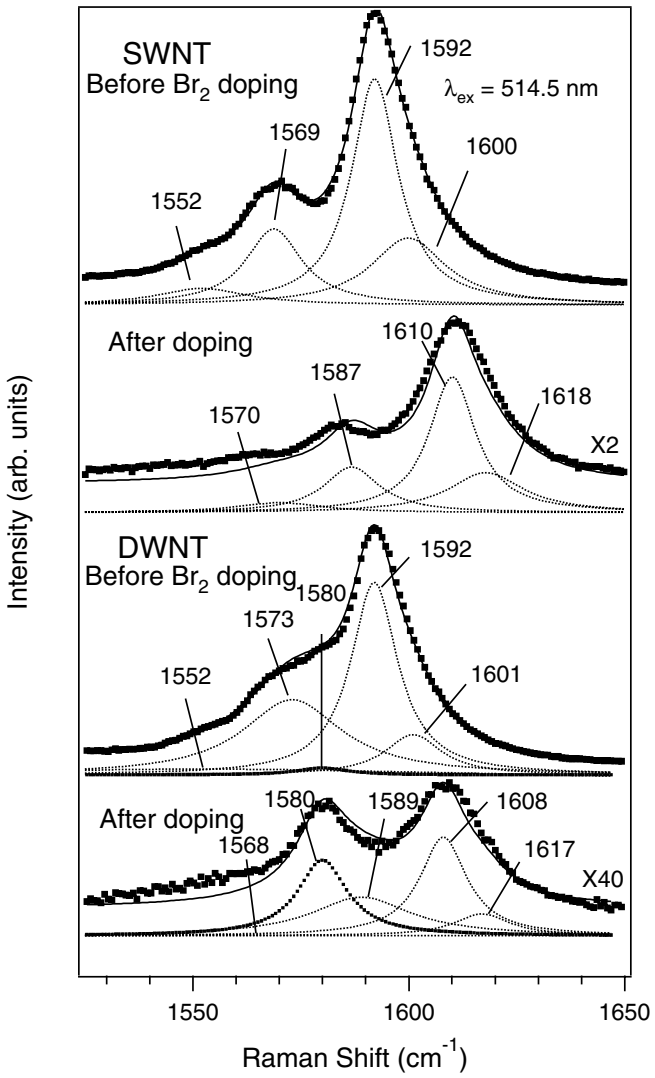

FIG. 2. Unpolarized Raman scattering spectra ($T = 300$ K) of DWNTs and SWNTs using 514.5 nm laser excitation. The upper lower pair of spectra are for the SWNT control (DWNT) sample. The thin solid line is the fit to the spectrum. Lorentzian components for the outer (inner) tubes are represented by dashed thin (dotted thick) lines.

resonance via the depression of the Fermi level by the bromine, which depopulates the initial states of the E_{22}^{s} transitions. A Lorentzian line shape analysis of the 1064 nm T-band spectra [Fig. 1(b)] also suggests that most of the charge is transferred from the bromine shell to the *outer* layer of the DWNT. For convenience, a single Lorentzian represents the three unresolved tangential modes in the strongly curved inner tube (1581 cm^{-1}) [3] and the outer tube (1590 cm^{-1}). After bromine doping (Fig. 1), the inner tube T band remains at 1581 cm^{-1}, whereas the outer tube T band vanishes (consistent with the results for the SWNT comparison sample).

The effects of bromine doping on the Raman T bands of the inner and outer carbon nanotubes can also be observed with 514.5 nm excitation (Fig. 2). The RBM region is omitted here, because the stretching frequency of bromine vapor at $\sim$320 cm^{-1} overlaps with the RBM frequencies of the inner tubes. The data of Fig. 2 were collected with a JY-ISA HR460 spectrometer (2 cm^{-1} resolution). The upper (lower) pair of the spectra show the SWNT (DWNT) results before and after doping. The details of the SWNT T band are better resolved with 514.5 nm excitation, fitted by a sum of four Lorentzians. The T band of the doped SWNT sample is well fit by a simple 18 cm^{-1} rigid up-shift of the undoped spectrum. We can fit the DWNT T band similarly: The pristine DWNT spectrum is fit by a relatively weak, unresolved T-band Lorentzian at 1580 cm^{-1} for the inner tube, plus the same four Lorentzians used to fit the 514.5 nm SWNT spectrum. After Br doping, the T bands shift and become very weak (note the 40× scaling of the signal). To fit the *doped* DWNT T-band spectrum, consistent with the analysis of the 1064 nm results, we simply superimpose the 1580 cm^{-1} Lorentzian band for the inner tube with an outer tube T band represented by the four-line fit to the *undoped* SWNT spectrum, but rigidly

up-shifted by 16 cm^{-1}. The T-band and R-band analyses indicate that the positive charge in our cylindrical molecular capacitor is deposited almost completely on the outer tube of the double-walled pair. Freezing the liquid bromine in the attached bulb with liquid N_2 only partially reverses the doping. Consistent with previous Raman scattering [4] and resistivity results [22] on bromine-doped SWNTs, the T band down-shifts to 1603 cm^{-1} (compared to 1592 cm^{-1} in pristine material). We did not try to fully reverse the doping; the sample remained at $\sim$27 °C while the bromine vapor was cryopumped; heating would most likely have driven ω_T closer to 1592 cm^{-1}. Interestingly, for alkali metal doping of SWNTs, some groups have reported a small initial up-shift of the T band, followed by the expected down-shift [7]. Our bromine-SWNT system, on the other hand, has a monotonic increase in the T-band frequency over the entire doping range.

We model the system as a three-layer cylindrical capacitor with the bromine anions forming a shell around the outer nanotube. The total energy contains three terms: the band structure energy of the inner and outer tubes and the electrostatic energy E^{es} of the trilayer charge distribution:

$$E = \sum_{i,k} E_i^{\text{inner}}(k) + \sum_{i,k} E_i^{\text{outer}}(k) + E^{es}. \tag{1}$$

The indices i and k label the occupied bands and wave vectors for the inner or outer tubes. For simplicity, we use a one-orbital tight-binding model with rigid bands and a nearest-neighbor π overlap $\gamma_0 = 2.90$ eV [20]. This model ignores the small $1/R^2$ curvature-induced band gap of $n \neq m$ tubes and nonrigid band effects. However, the model captures the primary physical effects relevant here: (i) the distinction between metallic and large band gap semiconducting tubes with radially dependent band gaps and (ii) the cylindrical electrostatics. The smallest diameter tube considered has $d = 0.63$ nm, approaching the size where rehybridization becomes relevant [23]. Subband filling is relatively modest, so a rigid band approximation is a reasonable starting point for the essential physics.

We assume that the excess charge on each shell is uniformly distributed in an infinitely thin wall at the nuclear radius of that shell. The resulting electrostatic energy of the triple-walled capacitor is

$$E^{es} = \frac{1}{2}\frac{e^2 L}{2\pi\varepsilon_0} n_{\text{inner}}^2 \ln\left(\frac{R_{\text{outer}}}{R_{\text{inner}}}\right) + \frac{1}{2}\frac{e^2 L}{2\pi\varepsilon_0} n^2 \ln\left(\frac{R_{Br}}{R_{\text{outer}}}\right), \tag{2}$$

where e is the electron charge, ε_0 is the permittivity of free space, L is the unit cell length of the outer tube, and n_{inner} (n) is the linear density of excess holes for inner tube (both tubes). R_{inner}, R_{outer}, and R_{Br} are the respective radii. We fix the charge per unit length in the Br shell (i.e., a theoretical dopant coverage with an attendant average charge per Br atom), and we minimize the total energy with respect to n_{inner}.

We consider DWNTs with inner and outer diameters in the ranges ($0.63 < d < 0.79$ nm) and ($1.3 < d < 1.5$ nm) [16]. The resulting wall indices are (**5**, **5**)@(**10**, **10**), (**5**, **5**)@(**13**, **7**), (**8**, **2**)@(14, 6), (6, 4)@(**10**, **10**), (6, 4)@(11, 9), (8, 0)@(12, 7), (7, 3)@(12, 8), (7, 2)@(13, 6), (8, 1)@(16, 2), and (9, 2)@(**11**, **11**), where the metallic tubes are in boldface. Two physical effects act in concert to segregate most of the holes onto the outer nanotube. First, the band gaps of the smaller diameter tubes tend to be larger, so they empty last. Second, the cylindrical geometry preferentially raises the electrostatic potential at the inner tube. Only the charge on the inner tube affects the potential difference between the two layers.

Figure 3 shows the results of the energy minimization. Two families of curves for n_{inner} vs n are obtained, one when the inner tube is semiconducting, and the other when it is metallic. The vertical scale (n_{inner}) is 10 times smaller than the horizontal scale (n); most of the positive

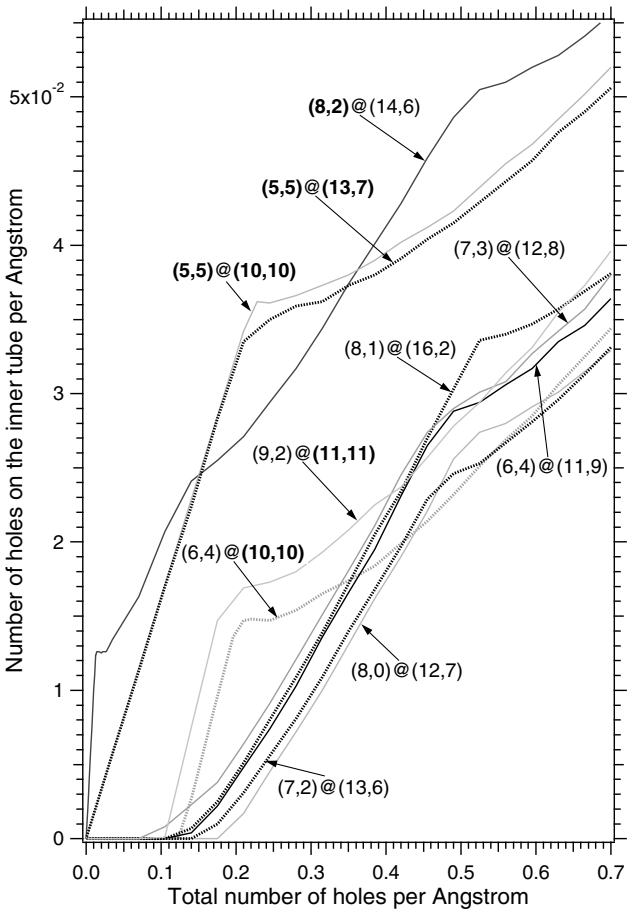

FIG. 3. Calculated number of holes per Å on the inner tube versus the total number of holes on the double-walled pair. Metallic tubes are in boldface. Alternation of grey and black curves is solely for clarity in distinguishing adjacent curves.

charge appears on the outer tube, in agreement with the experimental results. The lower family of curves is associated with two nested semiconducting tubes, except for (6, 4)@(**10**, **10**) and (9, 2)@(**11**, **11**), which have an outer metallic tube. In this family, the outer tubes alone are doped until the Fermi energy E_F cuts the first valence band in the inner tube and then a cusp appears. For the (6, 4)@(**10**, **10**) tube, the first cusp is at $n \approx 0.14$ holes/Å, where E_F first cuts the valence band of the (6,4) layer, and the next cusp occurs at $n \approx 0.21$ holes/Å, when E_F reaches the second valence band of the outer (**10**, **10**) layer.

Within the second (upper) family of curves, all of the inner tubes are metallic. The (**5**, **5**)@(**10**, **10**) and (**5**, **5**)@(**13**, **7**) are metallic pairs, so both tubes dope simultaneously. For (**8**, **2**)@(14, 6), the outer tube is semiconducting. Even though the inner tube dopes first in this case, the charge distribution rapidly begins to favor the outer tube as electrostatic effects begin to dominate. For the metallic (**5**, **5**)@(**10**, **10**) and (**5**, **5**)@(**13**, **7**) DWNTs, a cusp appears as E_F approaches the second valence band of the outer tube at $n \approx 0.22$ holes/Å, while for (**8**, **2**)@(14, 6) the cusp occurs at a smaller value of $n \approx 0.0126$ holes/Å, when E_F cuts the first valence band of the outer tube. Although some of these tubes are really small-gap semiconductors due to curvature-induced hybridization, the electrostatic effects dominate and therefore the small curvature-induced gap would have only a small effect on the overall charging behavior.

The charge transfer between the dopant (bromine) and the DWNT may be defined as the charge per host carbon atom transferred to the dopant, denoted as f. We can estimate f using the relation $\Delta\omega(\text{ cm}^{-1}) \approx 460 \times f$ obtained previously for the up-shift of the Raman-active E_{2g} modes (~ 1582 cm^{-1}) during electrochemical charging of graphite-H_2SO_4 [4]. For the saturation doped DWNT-bromine system, we observe a ~ 16 cm^{-1} up-shift of the T band in the *outer* tube relative to the undoped system (Fig. 2). Consistent with our tight-binding model, we assume that $\sim 90\%$ of these holes reside on the outer tube. Therefore, $f \approx 1/(29 \times 0.9) \approx 1/26$; saturation bromine doping creates one hole in the DWNT per 26 carbon atoms, or 0.6 holes/Å. E_F is then depressed by 1.2 to 1.4 eV [depending on (n, m)], uncovering states at the top of the third valence band of the semiconducting outer tubes. As a result, resonant Raman scattering from these outer tubes using 514.5 nm (or 2.41 eV) excitation should be dramatically reduced, in agreement with experiment. Theory (i.e., $<10\%$ of the charge on the inner tube) predicts a 1–2 cm^{-1} up-shift of the inner tube T band, near the limit of our experimental resolution.

Similar issues arise in higher stage index ($n > 3$) graphite intercalation compounds (GICs), where the bounding carbon layers adjacent to the charged intercalate layers are thought to contain most of the compensating charge. For example, optical reflectance studies of potassium GICs, showed that $\sim 90\%$ of the charge in the carbon layers was on the two bounding layers, and only 10% on the interior layers [24]. This charge distribution is similar to that obtained here in a double-tube cylindrical geometry, even though the electronic band structure for cylindrical graphene is very different from that of planar GICs. Recent results on DWNTs with BN outer walls and C inner walls [25] should exhibit a similar interplay of electrostatics and band filling, with an electrostatic favoritism to doping the outer layer.

This work was supported by the NSF NIRT program (DMR-0103585) and Penn State MRSEC (DMR-0213623). The Meijo group was supported by the Grant-in-Aid for Scientific Research (C) No. 145640545, and also the Japan Science and Technology Corporation.

*Author to whom correspondence should be addressed. Email address: pce3@psu.edu

[1] P. C. Eklund and G. L. Doll, Springer Ser. Mater. Sci. **18**, 105 (1992).
[2] M. S. Dresselhaus, G. Dresselhaus, and P. C. Eklund, *Science of Fullerenes and Carbon Nanotubes* (Academic, San Diego, 1996).
[3] M. S. Dresselhaus and P. C. Eklund, Adv. Phys. **49**, 705 (2000).
[4] A. M. Rao *et al.*, Nature (London) **388**, 257 (1997).
[5] W. A. Kamitakahara, J. Phys. Chem. Solids **57**, 671 (1996).
[6] U. D. Venkateswaran *et al.*, Phys. Rev. B **65**, 054102 (2002).
[7] L. Duclaux, Carbon **40**, 1751 (2002).
[8] T. Pichler *et al.*, Phys. Rev. B **67**, 125416 (2003).
[9] S. Bandow *et al.*, Chem. Phys. Lett. **337**, 48 (2001).
[10] S. Iijima and T. Ichihashi, Nature (London) **363**, 603 (1993).
[11] S. Iijima *et al.*, Chem. Phys. Lett. **309**, 165 (1999).
[12] B.W. Smith, M. Monthioux, and D. E. Luzzi, Nature (London) **396**, 323 (1998).
[13] B.W. Smith and D. E. Luzzi, Chem. Phys. Lett. **321**, 169 (2000).
[14] K. Hirahara *et al.*, Phys. Rev. Lett. **85**, 5384 (2003).
[15] Y. Maniwa *et al.*, J. Phys. Soc. Jpn. **72**, 45 (2003).
[16] S. Bandow *et al.*, Phys. Rev. B **66**, 075416 (2002).
[17] A. M. Rao *et al.*, Science **275**, 187 (1997).
[18] H. Kuzmany (to be published).
[19] Z. X. Jin, G. Q. Xu, and S. H. Goh, Carbon **38**, 1135 (2000).
[20] H. Kataura *et al.*, Synth. Met. **103**, 2555 (1999).
[21] R. Saito, G. Dresselhaus, and M. S. Dresselhaus, Phys. Rev. B **61**, 2981 (2000).
[22] R. S. Lee *et al.*, Nature (London) **388**, 255 (1997).
[23] X. Blase *et al.*, Phys. Rev. Lett. **72**, 1878 (1994).
[24] M. H. Yang and P. C. Eklund, Phys. Rev. B **38**, 3505 (1988).
[25] W. Mickelson *et al.*, Science **300**, 467 (2003).